Landsc Ecol (2022) 37:3179–3199
https://doi.org/10.1007/s10980-022-01535-4

RESEARCH ARTICLE

UAVs improve detection of seasonal growth responses during post-fire shrubland recovery

J. J. van Blerk · A. G. West · J. Smit · R. Altwegg · M. T. Hoffman

Received: 8 February 2022 / Accepted: 22 September 2022 / Published online: 2 October 2022

Abstract (1) We monitored post-fire shrubland recovery responses to changes in rainfall seasonality using a multi-year field experiment in the Cape Floristic Region (CFR) of South Africa. A primary objective was to test the utility of UAVs for monitoring ultra-fine-scale vegetation changes in the early post-fire context. (2) By comparison with detailed ground-based measurements, we showed that UAVs improved detection of integrated community growth responses, given that the appropriate relative radiometric normalisation techniques were applied to repeated imagery data. UAVs supported ground-based findings and, moreover, helped to identify previously undetected growth form responses. However, due to the limitations in detecting species-specific demographic changes, UAVs could not completely replace ground-based measurements. (3) Our combined UAV-based and ground-based monitoring approaches indicated strong coupling between post-fire shrubland recovery and seasonal rainfall patterns in the CFR but also demonstrated that sensitivity to rainfall seasonality could differ between neighbouring shrubland communities occurring on different soil types. (4) The careful integration of UAV-based and ground-based monitoring approaches provided the fullest understanding of early post-fire shrubland recovery patterns.

Keywords UAV · Pseudo-invariant features · NDVI · Multispectral · Radiometric normalisation · Remote sensing · Post-fire · Shrubland · Rainfall · Seasonality

Supplementary Information The online version contains supplementary material available at https://doi.org/10.1007/s10980-022-01535-4.

J. J. van Blerk (✉) · A. G. West
Department of Biological Sciences, University of Cape Town, Private Bag X3, Rondebosch 7701, South Africa
e-mail: jvanblerk@gmail.com

J. Smit
Department of Geomatics, University of Cape Town, Private Bag X3, Rondebosch 7701, South Africa

R. Altwegg
Centre for Statistics in Ecology, Environment and Conservation, Department of Statistical Sciences, University of Cape Town, Private Bag X3, Rondebosch 7701, South Africa

M. T. Hoffman
Plant Conservation Unit, Department of Biological Sciences, University of Cape Town, Private Bag X3, Rondebosch 7701, South Africa

Introduction

Monitoring vegetation change is central to understanding dynamic, disturbance-prone ecosystems. The Mediterranean-type shrublands of the world are uniquely dynamic ecosystems due to periodic wildfires which clear standing vegetation and initiate new cycles of emergence, growth, and succession

(Rutherford et al. 2011; Keeley 2012). Effective methods of change detection are needed to gain a better understanding of these dynamic recovery processes as well as to quantify their sensitivity to climate change, which is expected to impact these ecosystems (Odum 1969; Grime et al. 2000; Kröel-Dulay et al. 2015). Early post-fire recovery processes are thought to be especially sensitive to post-fire weather, potentially amplifying the impact of climate change in shrubland ecosystems. For example, potential changes in rainfall amount and seasonality (Altwegg et al. 2014) could affect post-fire recovery dynamics through complex changes in species recruitment, survival, reproduction, and competition (Moreno et al. 2011; West et al. 2012; Nelson et al. 2013; van Blerk et al. 2021a, b) with potential consequences for vegetation trajectories and community structure over longer time scales (Keeley et al. 2005; Moreno et al. 2011; Bond and van Wilgen 2012). Indeed, the importance of understanding the sensitivity of early post-fire recovery processes (e.g., ± first 3 years) has long been recognised because this formative period may shape mature ecosystem states.

Despite the importance of monitoring early-post fire recovery processes, the high diversity and small size and of recovering plants requires an exceedingly detailed, fine-scale monitoring approach to detect community changes effectively. This limits either the spatial coverage or resolution of traditional, ground-based, post-fire studies (Gitas et al. 2012). Furthermore, access to recently burned sites is typically limited by parks management due to the sensitivity of these landscapes to trampling. A significant challenge for ecologists is describing integrated community responses to climate change because many species that make up early post-fire plant communities are difficult to detect and measure. This has resulted in most ground-based post-fire studies focusing on key, easily detectable species, although some attempts at recording comprehensive community changes during early post-fire recovery have been made (e.g., Rutherford et al. 2011). Satellites provide multi-spectral imagery of increasing spatial and temporal resolutions which is helpful for monitoring recovery patterns over large spatial scales, yet the resolution of available satellite imagery is still generally too coarse for the detection of ultra-fine scale community changes during early years (i.e., first 3 years) of post-fire recovery (Aplin 2005; Gitas et al. 2012; Wilson et al. 2015; Pádua et al. 2020). Very low vegetation cover during this time generally limits the ability of satellite imagery to isolate vegetation signals from background signals. This imposes a strong limit to the resolution of vegetation changes detectable during this sensitive time-period. Taken together, the low detectability of post-fire vegetation activity and innate community complexity has made it challenging for ecologists to quantify complex, patch and landscape level community dynamics in post-fire landscapes. However, the introduction of unmanned aerial vehicles (UAVs) in the last decade has offered the possibility of detecting ultra-fine-scale vegetation patterns and changes over larger spatial extents (Anderson and Gaston, 2013; Cunliffe et al. 2016; Baena et al. 2017; Sankey et al. 2018; Waite et al. 2019; Fernández-Guisuraga et al. 2022). This could offer key insights into the sensitivity of shrubland community recovery processes to changes in climate.

We report new findings from our recent post-fire research in the Cape Floristic Region (CFR), South Africa, where we monitored ultra-fine-scale shrubland recovery responses to changes in rainfall seasonality during the first 3 years after fire. The degree of coupling between rainfall seasonality patterns and post-fire recovery processes in the CFR shrublands is not well understood. Regional vegetation-climate relationships are obscured by complex interactions between fire-cycles, climate seasonality, edaphic heterogeneity, and functional specialisation within distinct shrubland communities (Bergh et al. 2014; Bradshaw and Cowling 2014). Disentangling these processes is thus of great importance and requires effective methods of observation and change detection. Our multi-year field experiment combined traditional ground-based and UAV-based monitoring approaches to capture ultra-fine-scale vegetation changes in response to varied rainfall seasonality, providing a unique opportunity to test and compare these methods in the post-fire context.

Previous analysis of the ground-based measures of demography, growth and productivity revealed that changes in rainfall seasonality had the capacity to affect post-fire successional trajectories and species dominance patterns over multi-year time scales (van Blerk et al. 2021a, b). Additionally, it was found that recovery responses to rainfall differed between neighbouring Fynbos and Renosterveld shrublands and were potentially mediated by edaphic factors (van

Blerk et al. 2021a, b). Post fire recovery in nutrient-impoverished Fynbos was decoupled from rainfall seasonality patterns compared to the neighbouring Renosterveld community, occurring on moderately fertile soils (van Blerk et al. 2021a, b). Entrenched differences in habitat preference and resource-use patterns between shrubland communities could have important implications for how these shrublands are expected to respond to changes in rainfall over short and long-term time scales. While ground-based measurements were able to detect fine-scale community and species responses to post-fire rainfall, they were extremely time-consuming and required hundreds of hours in the field and tens of thousands of individual plant measurements to monitor changes in every plant occurring on 24*16 m^2 plots over 3 years (van Blerk et al. 2021a, b). There were also significant challenges in quantifying complex plant canopy shapes and thus plant sizes were measured based on their widest and highest points. In growth forms which were particularly challenging to measure, vegetation changes were monitored using estimations of percent cover over time. The inherent limitations of ground based monitoring highlighted the need for more efficient monitoring techniques.

Here, we test the performance of multispectral, UAV-derived imagery data, which was captured over experimental, post-fire plots concurrently to ground-based measurements. Our study demonstrates a practical approach to using UAVs for monitoring fine-scale, post-fire vegetation change for the non-remote sensing specialist. By comparison with ground measurements, we investigate the extent to which UAV-based measurements can augment or replace ground-based measurements and assess whether UAV data modifies, supports or rejects previous conclusions of the impacts of rainfall seasonality on post-fire CFR shrubland recovery.

Methods

Study site and multi-year post-fire rainfall experiment

We monitored post-fire vegetation recovery over 3 years at the Drie Kuilen Nature Reserve (33.5805° S, 20.0332° E) in the Western Cape of South Africa. The vegetation of this semi-arid region (< 300 mm MAP) includes fire-prone shrublands: Matjiesfontein Shale Renosterveld and Langeberg Sandstone Fynbos (Mucina and Rutherford 2006).

This site was used to test the impact of post-fire rainfall seasonality on early post-fire recovery using a field rainfall manipulation experiment. We conducted our study in neighbouring Fynbos and Renosterveld sites located within a kilometre of each other (with < 200 m altitude difference), either side of a distinct ecotone. We monitored 12 permanent 16 m^2 plots within each site (Fig. 1) after a controlled burn in May 2016. At each site, half of the post-fire plots received natural seasonal winter rainfall (controls) and the other half received a 'reduced rainfall seasonality' treatment over the duration of the experiment. Reduced rainfall seasonality treatment was achieved by capturing and storing ~ 50% winter rain above plots using clear roofing strips (i.e. reducing winter rainfall) and irrigating the same plots with this captured rainfall during the hottest summer months (3 × 30 mm irrigation events: Jan × 1, Feb × 1, Mar × 1). The net effect of this was to redistribute a portion of the winter rainfall onto plots during the typically hot dry summers without changing net annual rainfall amounts. This treatment was designed specifically to test the effects of rainfall timing in the post-fire environment. See van Blerk et al. 2021a, b for a detailed description of the experimental setup and seasonal soil moisture effects.

Multispectral imagery collection using UAVs

Starting in February 2017, aerial imagery of Fynbos and Renosterveld sites was captured twice a year using UAVs (DJI Phantom 3 Professional—https://www.dji.com) and a mounted multispectral camera (Parrot sequoia—https://www.parrot.com). Unfortunately, pre-first summer imagery was not captured due to logistical issues, limiting the UAV data from Feb 2017 to May 2019. Experimental rain capture roofs were temporarily removed from plots before UAV surveys. The Parrot sequoia multispectral camera was mounted onto the DJI Phantom 3 Professional with a Parrot Sequoia Mount Kit. On each survey date images were captured from a height of 20 m during a 2D grid flight path with > 80% overlap. Survey flight paths were programmed using AtlasFlight (https://micasense.com) software. The Parrot sequoia captured red (640–680 nm) and near infrared (NIR) (770–810 nm) bands using multispectral sensors

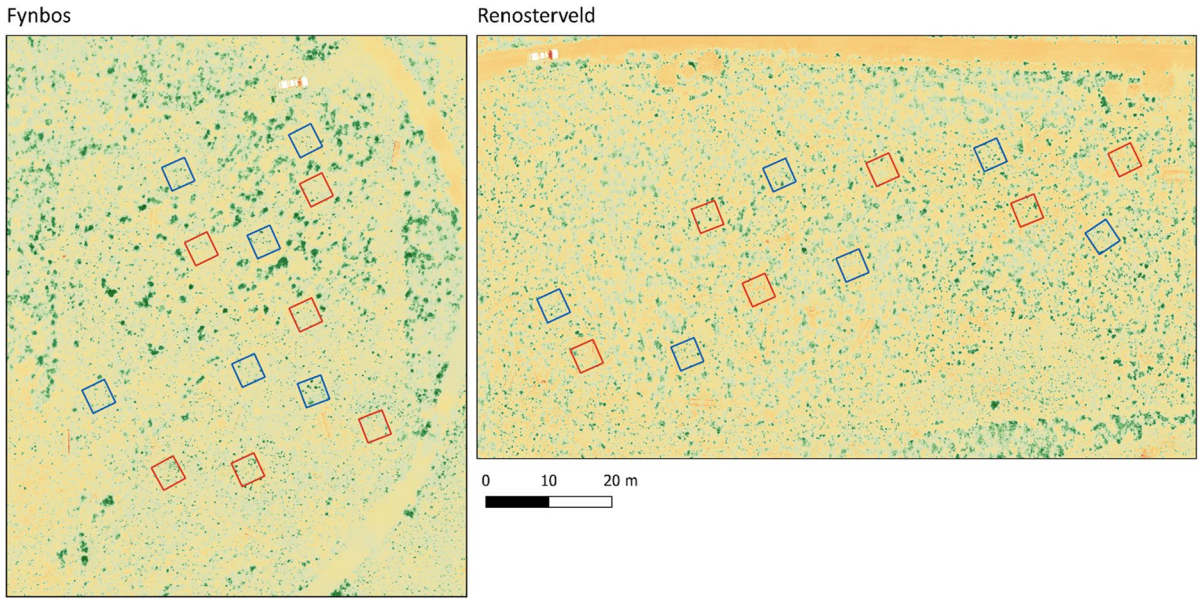

Fig. 1 NDVI orthomosaic image layers covering the post-fire rainfall seasonality experiment in Fynbos and Renosterveld field sites. Pixel colour scale represents NDVI-1 (red): 1 (green). Red squares indicate the position of 16 m^2 focal plots with natural winter rainfall (controls) and blue squares indicate the position of plots with reduced rainfall seasonality. Repeated orthomosaic layers were obtained at each site on Nov 2016, Feb 2017, Oct 2017, Apr 2018, Oct 2018, May 2019

and also captured RBG (Red, Green, Blue) images. Repeated UAV surveys were always conducted as close to midday as possible to reduce shadows around vegetation. UAV surveys were also conducted on days with 0% cloud cover. Flight times did not exceed 25 min due to battery-life limitations.

Single-band red and NIR images were calibrated using standard Pix4D Mapper (https://www.pix4d.com) software calibrations. These included (i) camera corrections (e.g. vignetting, ISO, dark current etc.), (ii) radiometric calibration panel reflectance values and (iii) sunshine sensor data. Immediately before and after surveys, images of a MicaSense calibrated reflectance panel (https://support.micasense.com) and 18% grey cards were captured (Fig. S1). This allowed for the Pix4D Mapper image-processing software to apply radiometric calibrations to single band images (e.g. red and NIR) via the empirical line method. The Pix4D software used only a single radiometric target to perform image corrections, but the other target served as a backup in case of calibration images being over-exposed. Additionally, a Sunshine Sensor module (https://www.parrot.com) recorded incoming solar irradiance during surveys to account for changes in solar intensity. The sunshine sensor module was fitted to the Phantom 3 Professional using a Parrot Sequoia Mount Kit.

For each survey date, corrected and calibrated red and NIR images were orthorectified and converted into composite, single-band orthomosaic images which covered the full area of the sites. Orthomosaic layers covered ~ 2.7 and ~ 3.2 acres for Fynbos and Renosterveld sites respectively with a ground sampling distance of < 2.5 cm). Red and NIR orthomosaic images were automatically aligned by Pix4D software using the known lens offset positions on the camera. Single-band orthomosaic layers were then converted into the normalized difference vegetation index (NDVI) (Fig. 1).

$$NDVI = \frac{NIR - RED}{NIR + RED} \quad (1)$$

NDVI is a commonly used vegetation index in remote sensing (Tucker 1979), providing pixel-by-pixel indication of photosynthetic activity (or

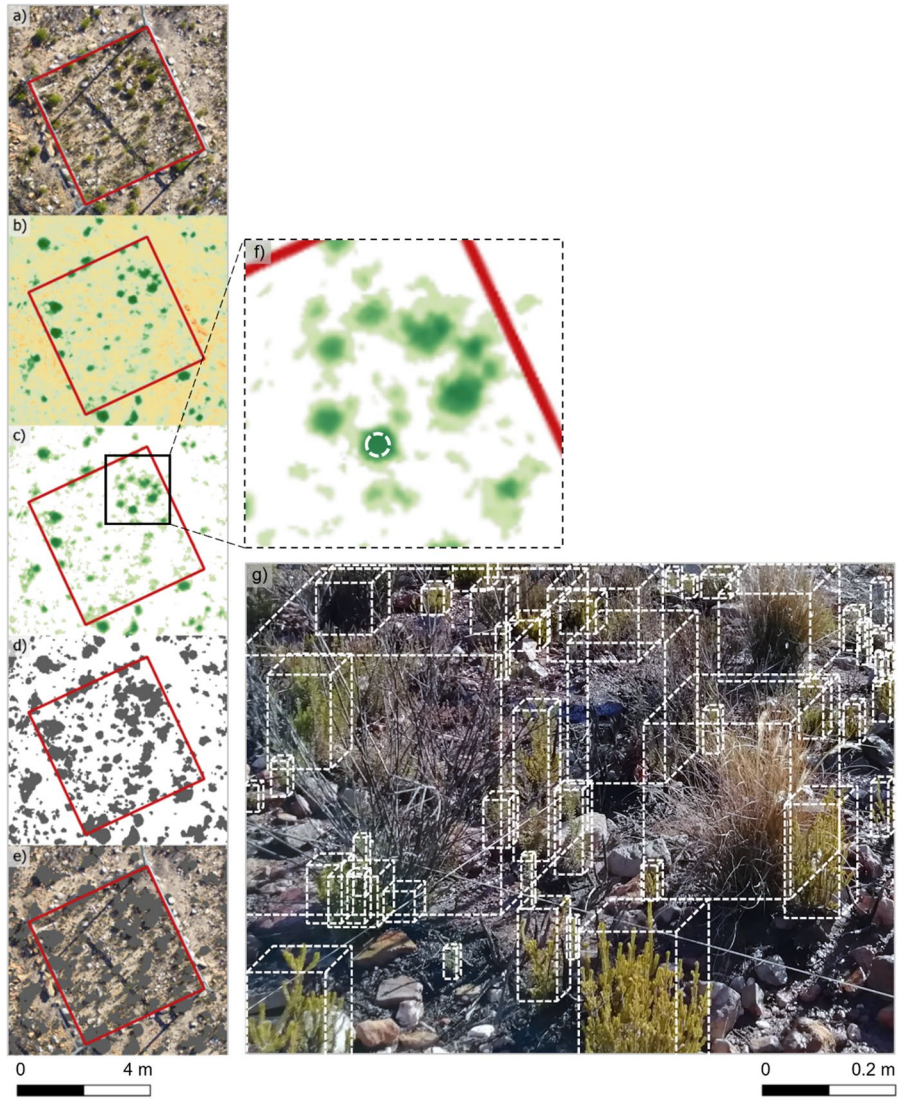

Fig. 2 **a** RGB orthomosaic image showing vegetation and soil for a single 16 m^2 post-fire focal plot. **b** Plot NDVI (including background and vegetation pixels) with pixel colour values ranging from − 1 (red) to 1 (green). **c** Vegetation NDVI after applying an image segmentation threshold of NDVI > 0.2 (i.e., excluding background NDVI pixels). **d** Vegetation area cover (UAV). **e** Overlay of vegetation area cover polygons on RGB images for visual comparison. **f** Shrub NDVI derived from fixed polygon (white dashed circle) set within the canopy of an identifiable shrub. **g** Ground-based volume measurements showing the complexity of plant cover and overlap between plant canopies

greenness) within repeated images. NDVI makes use of the high absorption of red light in leaf material and a high reflectance of near infrared (NIR) light to differentiate plants from non-photosynthetic materials within an image. Studies have shown the effectiveness of NDVI in estimating vegetation recovery in post-fire environments with variable soil types (Veraverbeke et al. 2012).

Repeated orthomosaic NDVI layers were produced for Fynbos and Renosterveld sites on 5 separate survey dates (i.e. Feb 2017, Oct 2017, Apr 2018, Oct 2018, May 2019). In addition to NDVI orthomosaic images, RBG orthomosaic images were also generated for comparison at each time step.

Measuring post-fire vegetation changes

UAV-based variables

We used a combination of QGIS (QGIS Development Team, 2009 http://qgis.org) and R (R Core Team 2020. https://www.r-project.org) to extract and summarise pixel values from the multispectral imagery over the 5 survey dates. For both the Fynbos and Renosterveld site, polygons (drawn in QGIS) were used to delineate the 16 m^2 focal plots in the series of aligned RGB (Fig. 2a) and NDVI (Fig. 2b) orthomosaic layers over time. RGB image layers were used as a guide for choosing the correct positioning of polygons. The

Table 1 Summary of the measured variables used to track post-fire vegetation recovery

UAV-based	
Plot NDVI	• Mean of all NDVI pixel values within plot including ground and vegetation pixels. $-1 \leq NDVI \leq 1$.
Vegetation NDVI	• Mean of all NDVI pixel values within plot which are classified as vegetation after image segmentation. $0.2 \leq NDVI \leq 1$.
Area cover (UAV)	• 2D area of polygons within plot which are classified as vegetation after image segmentation (m^2).
Shrub NDVI	• Mean of NDVI pixel values within polygon delimiting the core canopy pixels of individual shrubs. $0.2 \leq NDVI \leq 1$.
Ground-based	
Height	• Distance from ground to tallest point on plant (m) [We report changes in mean vegetation height per plot.]
Area cover (G)	• Width × length set to the widest points of each plant (top-down 2D) (m^2). [We report changes in the summed area cover of all plants within a plot.]
Volume	• *Height* × *Area cover (G)* (m^3). [We report on changes in the summed volume of all plants within a plot.]
Plant count	• Number of plants occurring within plot.

bases of the upright steel poles in the corner of each focal plot served as points of orientation for alignment. The exact_extract() function was used to summarise NDVI pixel values from within plot polygons.

We used a simple NDVI image thresholding technique to isolate vegetation pixels from the soil pixels within the NDVI orthomosaic images (Fig. 2c). This entailed removing all pixels from NDVI orthomosaic layers below a chosen NDVI threshold value < 0.2, resulting in vegetation-specific spectral data for each plot (Fig. 2c). The presence/absence of pixels then corresponded with vegetation cover versus no vegetation cover in images respectively, allowing for the quantification of high-resolution area cover per plot (Fig. 2d). Area cover was measured by multiplying the number of pixels above the threshold of 0.2 NDVI by the squared pixel area. Overlaying the threshold images onto RGB images allowed for a visual comparison of threshold area and visible vegetation patches (Fig. 2e). The chosen NDVI threshold value was visually adjusted until it most successfully corresponded to vegetation patches. Because NDVI pixel density histograms were unimodal, we did not attempt to use automatic thresholding algorithms (e.g. Otsu 1979). Instead, we chose to manually select and adjust thresholds based on available pixel information. We also considered automatic edge detection methods (e.g. level setting) to calculate the area of vegetation within NDVI images (e.g. Ghazal et al. 2015) but due to the computational complexities of such a method, we settled with our simpler, more accessible approach. Species-level data was extracted for a single dominant and sufficiently, isolated species at each site (i.e., *Agathosma capensis* in Fynbos and *Passerina obtusifolia* in Renosterveld) using fixed polygons delimiting core pixels within shrub canopies (Fig. 2f).

Ground-based variables

Detailed plant demographic surveys were conducted at the same time as UAV-based surveys. Demographic surveys included counting and measuring the area and height of every plant occurring within each of the 16 m^2 focal plots (Fig. 2g). Over 60,000 individual ground-based measurements were made over the duration of the experiment starting in Nov 2016 (van Blerk et al. 2021a, b). At the Fynbos site graminoid growth forms (primarily grasses and sedges) were measured using estimated % cover because cover was too high to distinguish between different individual plants. Estimated % cover was later converted to area cover and volume before analysis, using simple conversions. In this study we report only the vegetation changes where both UAV and ground-based measures were made (i.e., Feb 2017–May 2019). See Table 1 for a full summary of the types of data used in our study.

Relative radiometric normalisation (RRN) of NDVI orthomosaic images

Tracking pseudo-invariant features (PIFs) within NDVI image layers to assess temporal radiometric distortion in repeated imagery

While we followed the recommended protocols for the collection and calibration of red and NIR images

using the Parrot Sequoia and Pix4DMapper, we found that additional steps were required to obtain temporal radiometric stability in repeated orthomosaic NDVI images. We achieved this by applying additional radiometric corrections directly to NDVI orthomosaic images. The radiometric stability of the NDVI pixel values in repeated orthomosaic image layers was investigated by tracking the variation in pseudo-invariant features (PIFs) within the NDVI image layers over time. PIFs are commonly used for the relative radiometric normalisation of time-series data which is often required for accurate land cover change detection (Bao et al. 2012; Zhou et al. 2016). Here PIFs were considered to be landscape features or objects within images which were not expected to vary over time in terms of their NDVI value, regardless of factors such as season or time after fire. PIFs were thus intended to reveal variation in the images which was not driven by real landscape changes, but rather by artifacts of the imagery acquisition process. PIFs included a trackable low-value NDVI feature and a high-value NDVI feature. PIFs were tracked over time using polygons in fixed positions aligned with the orthoimages. A combination of low and high value PIFs were necessary to monitor image stability over the full spectrum of possible pixel values. This is because temporal radiometric distortion in pixel values over repeated images was not necessarily equal across all pixels and could arise from the compression or expansion of NDVI scale rather than image-wide pixel value shifts.

Selection of pseudo-invariant features

We selected bare soil patches as low NDVI value PIFs (Fig. 3a) because we assumed that soil NDVI values should not change over time and should have consistent, low NDVI value. The central pixels of dense, unburnt, off-plot, evergreen shrubs were selected as high NDVI value PIFs (Fig. 3a). We assumed that these pixels represented 100% evergreen leaf coverage with no soil pixels included. Using dense, evergreen vegetation polygons as PIFs could be problematic in some cases seeing that some seasonal variation in leaf NDVI might be expected. Ideally, PIFs should be inert, whereas vegetation NDVI values may vary. However, in this scenario, we argue that the central pixels of dense, evergreen, deep-rooted shrubs were likely to have minimal seasonal photosynthetic variation (van Blerk et al. 2021a, b) and were thus the best available option for a high NDVI value PIF. For each PIF, multiple polygons (>20) were chosen and tracked over time. Other potential approaches would be using PCA analysis to identify PIFs if they weren't easily identifiable (Du et al. 2002; Bao et al. 2012).

Image normalisation procedure

Relative radiometric normalisation (RRN) adjusted the pixel values of repeated image layers relative to the PIFs of the first image in the sequence (i.e. reference image). Pixel adjustment equations were modelled on the linear relationship between the PIF values of uncorrected and reference images (Fig. 3b), using the sum of least squares. Pixel values of uncorrected images were modified to their target values according to the formula

$$y_i = mx_i + c \tag{2}$$

where y = the value of a given pixel i within the corrected (radiometrically normalised) image, m = slope of the relationship between uncorrected PIFs and reference PIFs, x = the value of a given pixel i within uncorrected image, c = intercept of the relationship between uncorrected PIFs and reference PIFs.

Assessing the impact of relative radiometric normalisation using pixel density histograms

Image pixel density histograms (Fig. 4) demonstrated that compression of histogram peaks had occurred in some layers, even after applying pre-processing image calibrations based on the camera corrections, sunshine sensor and field radiometric calibration panels. The October 2018 Fynbos site imagery was most clearly affected by this phenomenon and displayed a compression of lower pixel values towards upper pixel values. This resulted in clearly elevated bare soil PIF pixel values (Fig. S2c) which corresponded with a large increase in plot NDVI relative to surrounding dates (Fig. S2a). Bare soil pixel values had a strong overall influence on mean plot NDVI because the majority of image pixels represented soil in the post-fire environment. Dense, evergreen vegetation PIFs in this layer were relatively stable (Fig. S2e). This indicated that the degree of the image radiometric distortion was not equal across the full range of NDVI

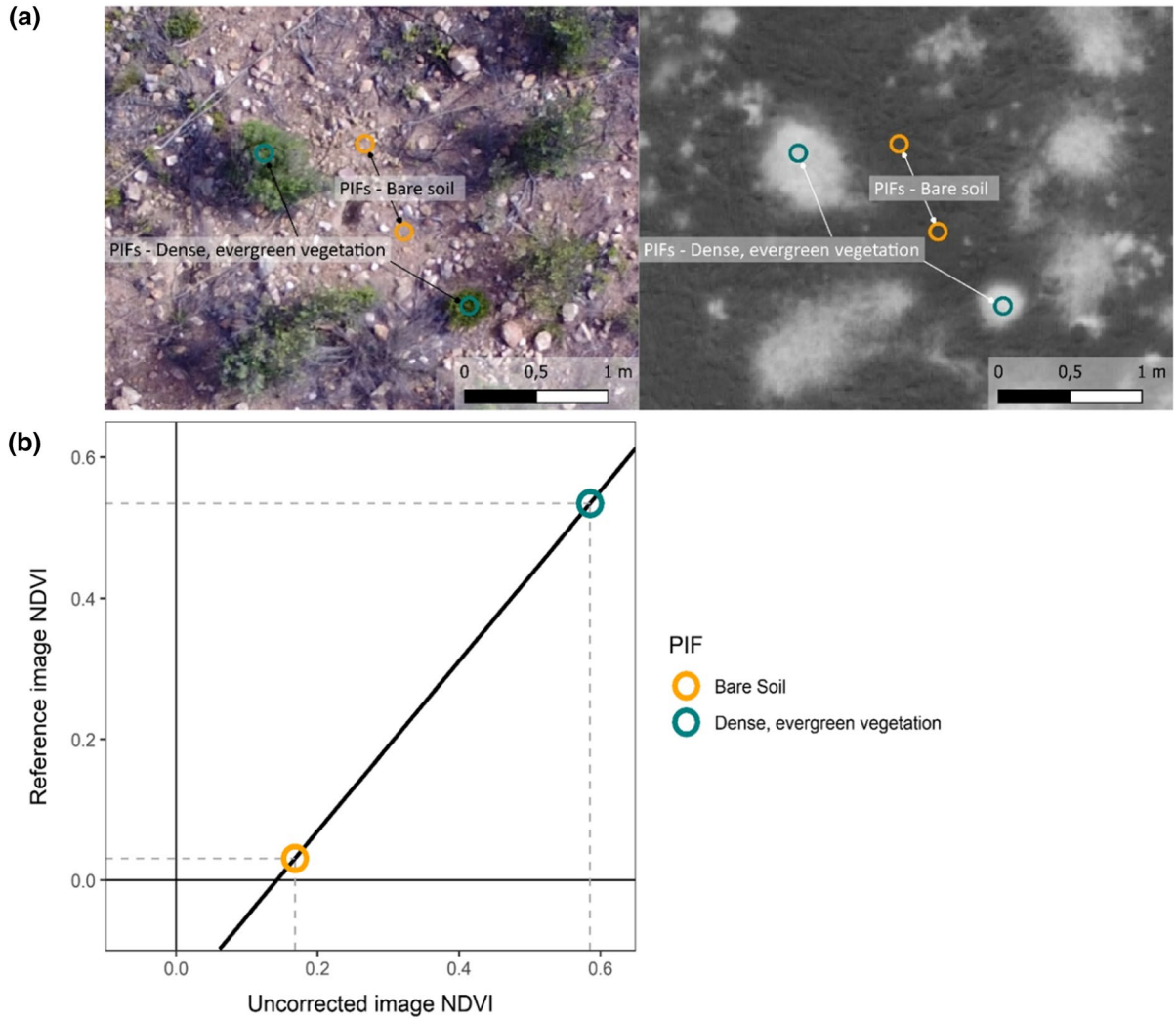

Fig. 3 **a** Example of pseudo-invariant features (PIFs) shown in RGB (left) and greyscale NDVI (right) images. Low NDVI value PIFs = bare soil (orange circles). High NDVI value PIFs = dense, evergreen vegetation (blue circles). **b** The relationship between Pseudo-Invariant-Features (PIFs) from an uncorrected image and reference image (i.e. first image in time-series). Dashed grey lines trace the PIF values to their positions on the x and y axes. Trendline is displayed in black and represents the line from which the normalisation equation is derived

values. Higher NDVI values were relatively unaffected by contrast problems which so clearly affected low NDVI values. In the Renosterveld image layers, radiometric distortion was less obvious, resulting in smaller peak differences over time.

Our RRN approach dramatically improved consistency of histogram peaks over time and resulted in the close alignment of PIFs across all repeated image layers (Fig. 4). Uncorrected image histograms were relatively similar to corrected image histograms at most time-periods in both sites with the exception of the October 2018 Fynbos site imagery where a large transformation effect is clearly visible (Fig. 4). It was apparent that matching dense, evergreen vegetation PIFs had a relatively small effect on the shape of histograms compared to the effect of matching bare soil PIFs, which strongly shifted histogram peaks. Importantly, even after matching

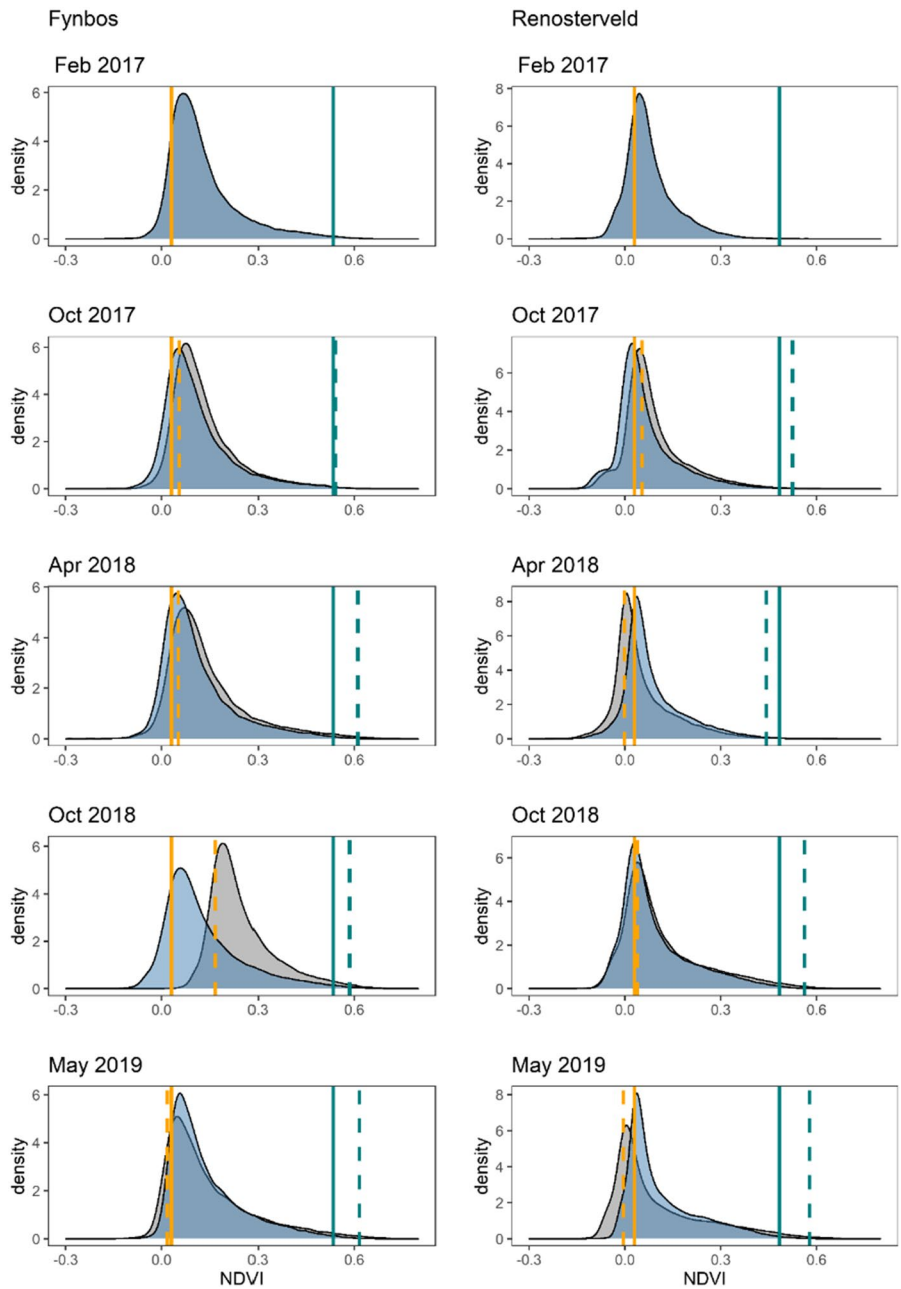

Fig. 4 NDVI pixel density histograms for uncorrected (grey) and corrected (radiometrically normalised) (blue) image layers. Solid vertical lines represent corrected PIF values for bare soil (yellow) and dense, evergreen vegetation (blue). Dashed vertical lines represent uncorrected PIF values

dense, evergreen vegetation PIFs over time, the density of the histograms toward upper NDVI values was still able to increase over time, indicating an increase in the fraction of vegetation relative to bare soil. In corrected imagery, plot NDVI patterns (Fig. S3a) did not include the large, spurious increases in mean plot NDVI and showed stable bare soil PIFs (Fig. S3c).

Visual assessment of the impact of relative radiometric normalisation

Isolating vegetation pixels from background pixels (i.e., image segmentation) using a common NDVI threshold was only successful with corrected (radiometrically normalised) imagery. This was confirmed using corresponding RGB images (Fig. 5). In

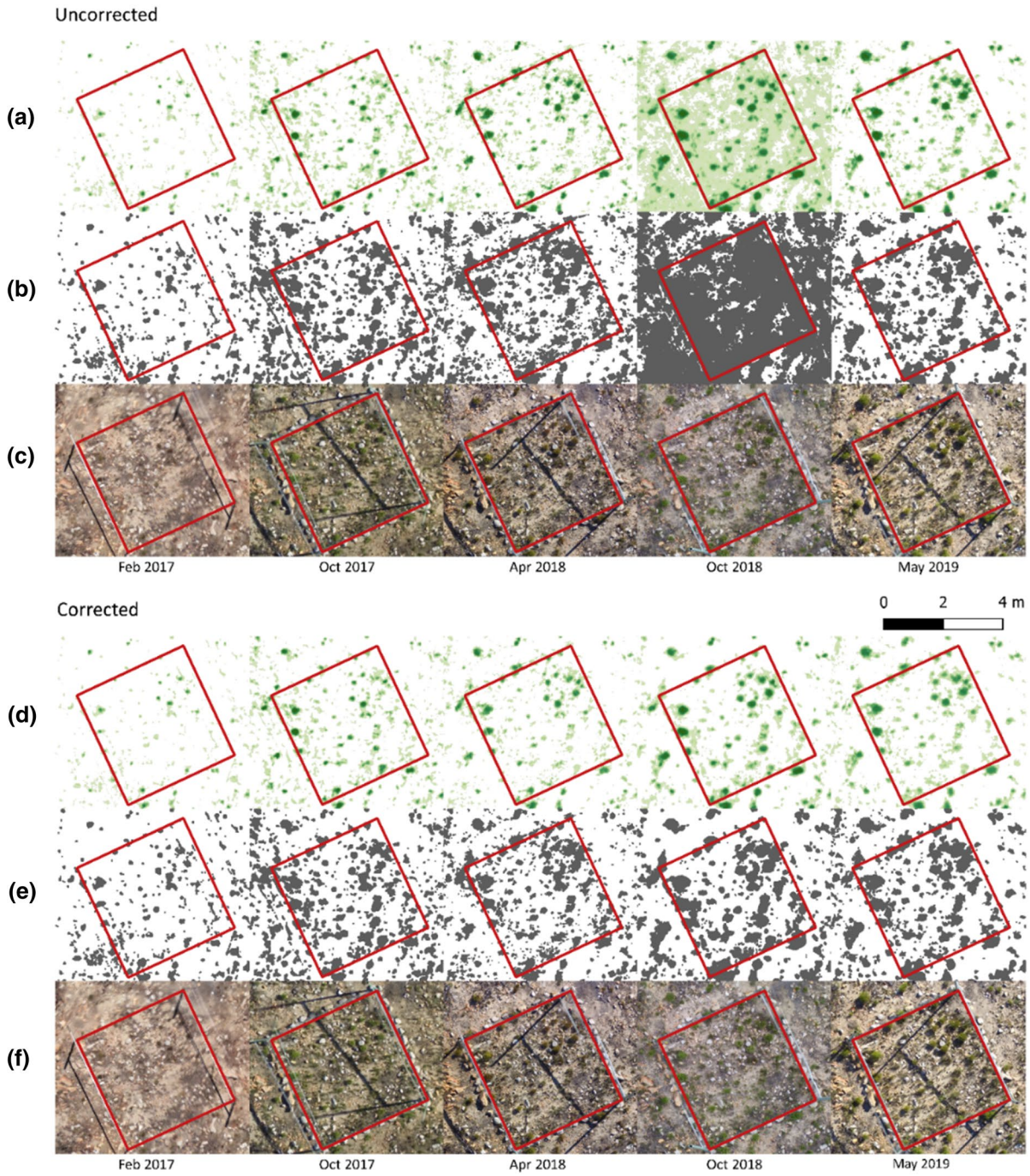

Fig. 5 Demonstration of the effects of radiometric noise on extracted data using a single focal plot in the Fynbos site. **a, d** Post fire changes in vegetation NDVI (NDVI > 0.2) within a 16 m^2 focal plot over time. White areas represent NA values while colour pixels represent NDVI values of vegetation. **b, e** Vegetation area cover polygons. **c, f** RGB images

uncorrected Fynbos images, radiometric distortion led to soil values being included above the chosen NDVI threshold during October 2018 (Fig. 5a–c), with obvious negative implications for area estimates and vegetation-specific signal estimates.

Analysis

Cross-referencing ground and UAV-based data

We assessed the general relationships between UAV and ground-based measures (e.g., Table 1) using a correlation matrix produced by the corrplot() package, including data from all survey dates, treatment groups and sites. Following this general comparison, we specifically investigated the relationship between *Area Cover (UAV)* and *Area Cover (G)*. This was intended to quantitatively assess the impact of RRN as well as to identify specific sources of disagreement between ground and UAV-based data. Identifying sources of disagreement was undertaken in two stages. First, we calculated the difference between *Area Cover (UAV)* and *Area Cover (G)* for each plot on each survey date to quantify the degree to which ground-measures over-estimated plot vegetation area cover relative to UAV-based measures. Here, over-estimation of *Area Cover (G)* relative to *Area Cover (UAV)* was expected because individual plant area measures on the ground were based on the widest points of plant canopies and because ground-based area totals included the sums of overlapping plants (Fig. 2g). An over-estimation index for each plot was then correlated against the dominance of specific species within plots to identify potential 'over-represented' species in the ground-based dataset. Species dominance was defined by the total contribution to ground-based plot area cover totals. Species with strong positive relationships between their dominance and the plot area cover overestimation were considered to be 'over-represented' in the ground-based data. We aimed to remove as few species as possible from our ground-based analyses, iteratively removing the largest contributors to area cover over-estimation until the relationship between *Area Cover (UAV)* and *Area Cover (G)* approached 1:1.

After removing over-represented species from ground-based datasets, we refit the linear relationship between *Area Cover (UAV)* and *Area Cover (G)* for each plot and used the residual standard error of this relationship as a measure of remaining disagreement between the two measures (not related to over-estimation). Residual SE (i.e., disagreement between measures) was then correlated with the level of dominance of different growth forms across plots to determine if specific growth forms were contributing to disagreement. We used the findings of these investigations to inform our analyses and refine our understanding of ground-based data.

Analysing the impact of altered rainfall seasonality on post-fire recovery

Due to post-fire recovery being a dynamic process of change, treatment effects (i.e., altered rainfall seasonality) were estimated on the *relative change* in response variables (Table 1) over discrete time periods (e.g. between Feb2017 and October 2017).

$$Relative\ change = \left(\log\left(Response\ variable_{t+1}\right) - \log\left(Response\ variable_{t}\right)\right)/\mathrm{Days} \quad (3)$$

where response variables = Table 1, $_{t}$ = survey date (1 = Feb2017; 2 = Oct2017; 3 = Apr2018; 4 = Oct2018; 5 = May2019), Days = number of days between t and t + 1.

The *relative changes* in response variables were contrasted between treatment groups (i.e. winter rainfall and reduced rainfall seasonality) and sites (Fynbos, Renosterveld). It was necessary to look at *relative change* over time because the instantaneous values of response variables at any single point in the time series could be more strongly related to values at previous time points (i.e. temporal autocorrelation) than to treatment effects over that time period. Therefore, isolating the effects of seasonality on response variables during discrete time periods had to account for potentially differing values between treatment groups or sites at the beginning of the set time period.

After converting response variables to *relative changes,* linear mixed effects models were used to estimate how the converted response variables were affected by rainfall seasonality (Winter rainfall (control), Reduced rainfall seasonality) over discrete seasonal periods since fire (W1 = Feb2017:Oct2017, S1 = Oct2017:Apr2018, W2 = Apr2018:Oct2018, S2 = Oct2018:May2019). Models also included Site

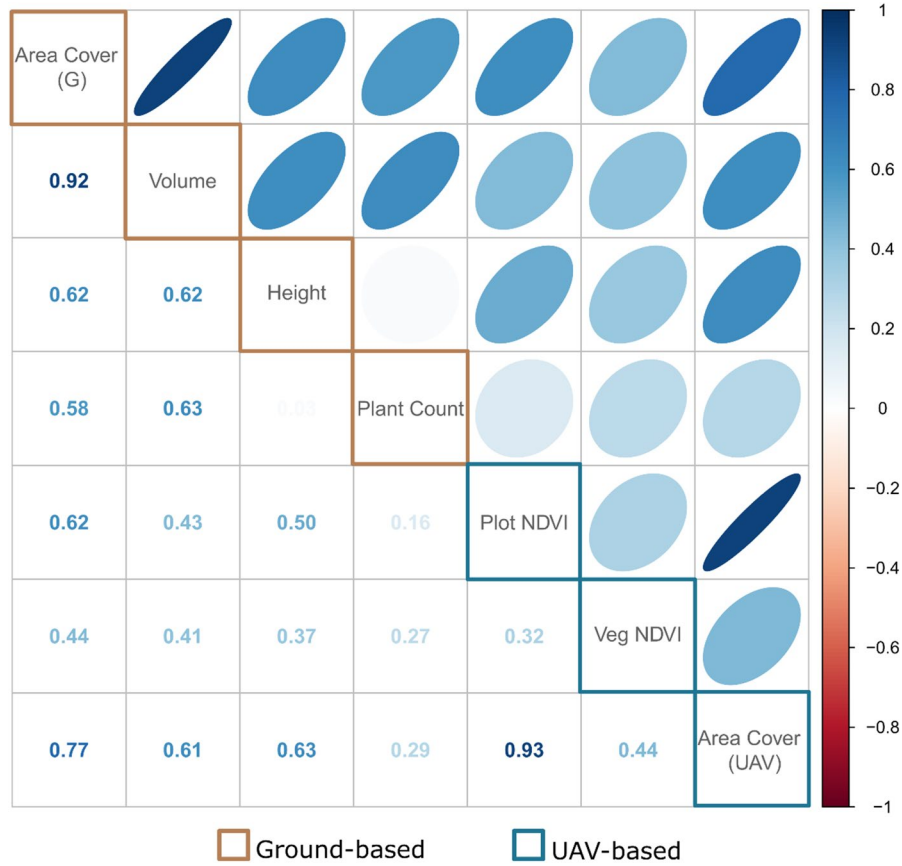

Fig. 6 Correlation matrix between ground and UAV-based variables. Numbers and ellipses represent the strength and direction of the correlation between variables. Non-significant correlations are not displayed

(Fynbos, Renosterveld) as an interaction term to compare the effects of rainfall between sites. We included the plot ID as a random effect due to the hierarchical structure of the data and to account for any uncontrolled, plot-specific differences in vegetation cover or community composition.

Results

General relationships between UAV-based and ground-based variables

Relationships between UAV-based vegetation variables

Over the duration of the experiment, *Plot NDVI* (Fig. 6) was strongly correlated with *Area Cover (UAV)* (Fig. 6), and was influenced to a lesser extent by *Vegetation NDVI* (Fig. 6). Changes in vegetation area cover are expected to have a stronger influence on plot NDVI signals in the post-fire environment, since initial post-fire cover is close to zero.

Relationships between ground-based vegetation variables

Strong relationships between *Area cover (G)* and *Volume* indicated that increases in canopy width and length had the largest influence on estimated plant volumes, rather than increases in *Height* (Fig. 6). This highlighted the potential importance of top down 2D top-down vegetation measures in describing post-fire recovery processes.

Relationships between UAV-based and ground-based vegetation variables

Of the remotely sensed variables, *Area Cover (UAV)* was most closely correlated to the ground-based measures, particularly with *Area Cover (G)* ($r = 0.77$, $p < 0.001$). *Plot NDVI* was weakly correlated with

ground-based measures on account of the vegetation signals being diluted by soil signals. *Vegetation NDVI* signals were not strongly correlated with any other UAV or ground-based variables (Fig. 6), indicating the unique characteristics of this measurement. *Vegetation NDVI* detected spectral changes within existing canopies (e.g. leaf health, leaf/canopy density) that were not captured by other measures.

Cross-referencing UAV and ground-based vegetation area cover measurements

By comparison with ground measurements, it was apparent that *Area Cover (UAV)* was strongly exaggerated in October 2018 for the Fynbos site if uncorrected imagery was used. RRN corrected this radiometric distortion and dramatically improved the agreement between *Area Cover (UAV)* and *Area Cover (G)* (Fig. 7a, b). The effect of RNN was most evident at the Fynbos site where temporal radiometric distortion was highest (e.g., October 2018 image layer) while comparatively little effect of RRN was observed in Renosterveld.

At both sites *Area Cover (G)* became progressively more overestimated relative to *Area Cover (UAV)* over time, as indicated by relationships with slopes larger than 1:1 (Fig. 7b). Here we assumed that corrected *Area Cover (UAV)* was the most accurate measure of top down 2D area cover. Confidence in UAV area cover estimates was best gained through visual comparison with RGB images. The over-estimation of *Area Cover (G)* relative to *Area Cover (UAV)* was explained by the presence of a small number of species which either had highly branched, diffuse canopies with highly reduced leaves or had high overlap between individuals (Table 2), thus disproportionately increasing ground-based area totals relative to UAV-based area measures. As these species grew, area cover measurements based on plant canopy wide points lead to progressively larger degrees of overestimation over time. These species were thus overrepresented in the ground-based measures over time relative to UAV-based measures. Removing these species from the ground-based data shifted the relationship between UAV and ground-based area cover estimates much closer to the 1:1 line in both sites (Fig. 7c).

Both before and after the removal of over-represented species, the relationships between *Area Cover (UAV)* and *Area Cover (G)* were found to be stronger at the Renosterveld site compared to the Fynbos site (using plot means or site means) (Fig. 7b, c) indicating a greater degree of disagreement between UAV and ground-based area cover estimates in Fynbos. Notably, the removal of over-represented species had limited impact on the strengths of the relationships between *Area Cover (UAV)* and *Area Cover (G)*.

In Fynbos, residual SE of the linear relationship between *Area Cover (UAV)* and *Area Cover (G)* for each plot over time (i.e. measure of disagreement) was strongly correlated with the relative dominance of graminoid growth forms across plots (Table 3). The most disagreement between *Area Cover (UAV)* and *Area Cover (G)* was present in plots with a higher graminoid dominance. This was consistent with the unique difficulties experienced when measuring graminoids using ground based methods at the Fynbos site. Due to the generally high proportion of graminoids at the Fynbos site ($31 \pm 5\%$ of total area), measurements of graminoids were made using % cover and later converted to area cover. This method of measurement thus had low accuracy compared to other individual plant measurements. Renosterveld had a lower overall graminoid component ($6 \pm 5\%$ of total area) and thus graminoids were measured individually. No correlations between growth form dominance and plot residual SE were found in Renosterveld. These findings indicate that ground-based estimates of graminoid area cover in Fynbos were too coarse for the detection of fine-scale, seasonal vegetation patterns. However, removing graminoids from the ground-based Fynbos dataset did not improve overall agreement between *Area Cover (UAV)* and *Area Cover (G)* in Fynbos and lead to strong underestimation of *Area Cover (G)* measures (data not shown). We considered the potential impacts of graminoid measurements in our final analysis. This included running our models with and without graminoids for the Fynbos site.

Impacts of rainfall seasonality on post-fire vegetation recovery

*Note that analyses were carried out using radiometrically normalised UAV-based data and 'refined' ground-based data (i.e., over-represented species removed).

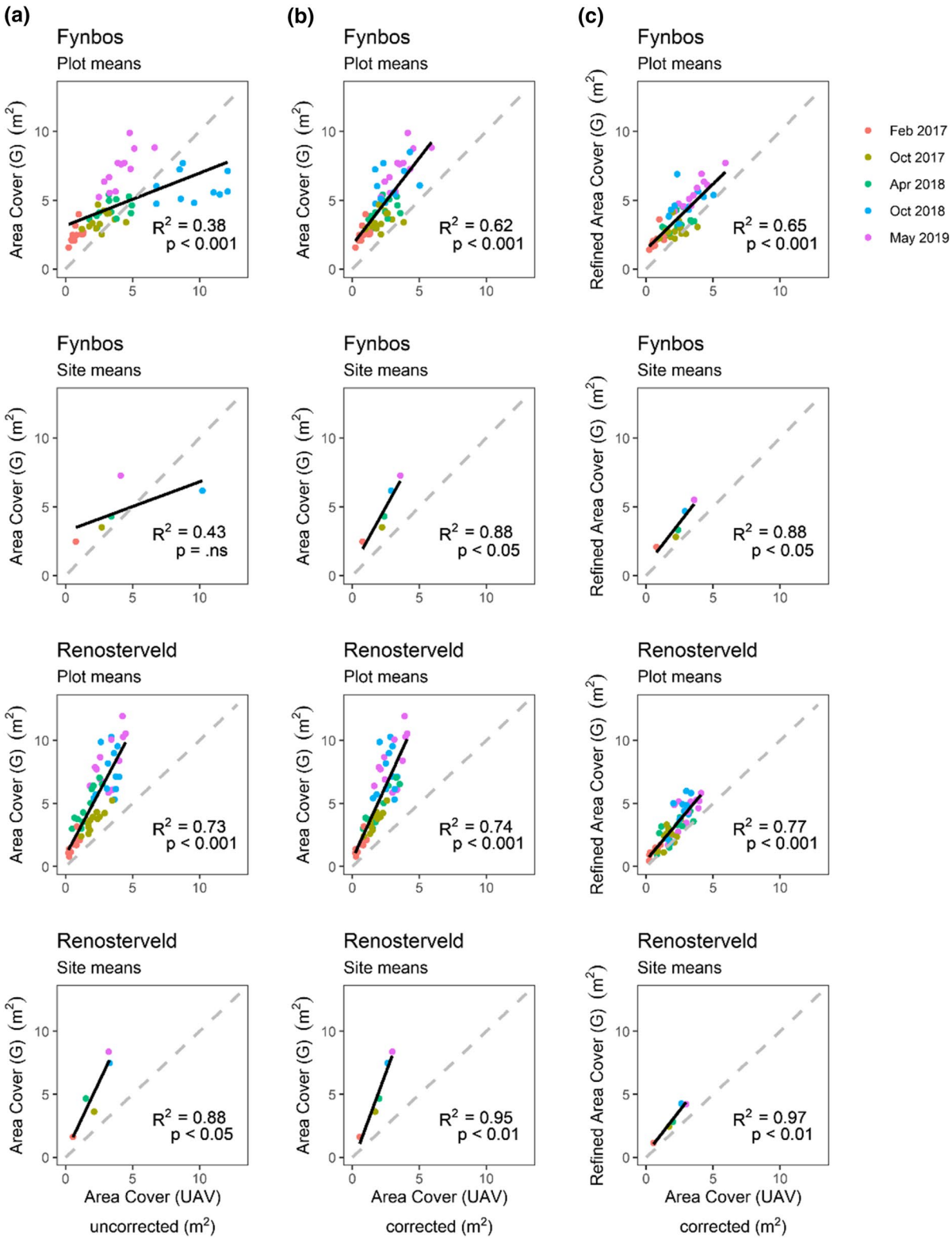
(a)
(b)
(c)
Fynbos
Plot means
Area Cover (G) (m²)
R² = 0.38
p < 0.001
Fynbos
Plot means
Area Cover (G) (m²)
R² = 0.62
p < 0.001
Fynbos
Plot means
Refined Area Cover (G) (m²)
R² = 0.65
p < 0.001
Feb 2017
Oct 2017
Apr 2018
Oct 2018
May 2019
Fynbos
Site means
Area Cover (G) (m²)
R² = 0.43
p = .ns
Fynbos
Site means
Area Cover (G) (m²)
R² = 0.88
p < 0.05
Fynbos
Site means
Refined Area Cover (G) (m²)
R² = 0.88
p < 0.05
Renosterveld
Plot means
Area Cover (G) (m²)
R² = 0.73
p < 0.001
Renosterveld
Plot means
Area Cover (G) (m²)
R² = 0.74
p < 0.001
Renosterveld
Plot means
Refined Area Cover (G) (m²)
R² = 0.77
p < 0.001
Renosterveld
Site means
Area Cover (G) (m²)
R² = 0.88
p < 0.05
Area Cover (UAV)
uncorrected (m²)
Renosterveld
Site means
Area Cover (G) (m²)
R² = 0.95
p < 0.01
Area Cover (UAV)
corrected (m²)
Renosterveld
Site means
Refined Area Cover (G) (m²)
R² = 0.97
p < 0.01
Area Cover (UAV)
corrected (m²)

◂**Fig. 7** Comparison of vegetation area cover (m^2) per 16 m^2 focal plot, obtained from ground-based measurements ('Area Cover (G)') and UAV-based measurements ('Area Cover (UAV)'). **a** Uncorrected 'Area Cover (UAV)' vs 'Area Cover (G)', including all species measured on the ground. **b** Corrected 'Area Cover (UAV)' vs 'Area Cover (G)' including all species measured on the ground. **c** Corrected 'Area Cover (UAV)' vs 'Refined Area Cover (G)', i.e., after the removal of overrepresented species (Table 2). Plot means include the measured vegetation area cover of each focal plot. Site means represent the mean of plot area cover measurements for each date. Black lines represent linear relationships between Area Cover (UAV) and Area Cover (G). Dashed lines represent the 1:1 relationship between variables

'Area cover (UAV)' and 'area cover (G)'

Post-fire changes in vegetation *Area Cover (UAV)* revealed strong winter-seasonality in Fynbos and Renosterveld under natural winter rainfall (dry summer) conditions (Fig. 8b). Here, significant increases in *Area Cover (UAV)* were restricted to winters (i.e., W1 and W2) whereas no change or declines occurred in summers (i.e. S1, S2). Both shrublands also displayed strong *Area Cover (UAV)* responses to reduced-rainfall seasonality treatments (Fig. 9b). Here, imposed reductions in the natural winter rainfall peaks (~ 50% rainfall reduction) reduced *Area Cover (UAV)* gains in winters, while alleviating summer droughts (~ + 90 mm rainfall) lead to *Area Cover (UAV)* gains in summer (Figs. 8b, 9b). Overall, our refined analysis showed a close coupling between UAV-based area cover estimates and post-fire rainfall patterns in both shrubland types (Fynbos and Renosterveld). This evidence was based on the combination of natural winter seasonality in control plots (Fig. 8b) (correlative evidence) and treatment responses (Fig. 9b) (causal evidence).

Ground-based estimates of vegetation area cover, *Area Cover (G)*, only detected strong winter seasonality and treatment responses in the Renosterveld site, while Fynbos was found to be relatively weakly coupled to rainfall seasonality patterns (Figs. 8f, 9f). This highlighted a clear disagreement between UAV-based and ground-based area cover estimates in the Fynbos site.

The removal of over-represented species (Table 2) from the ground-based analysis improved agreement between *Area Cover (UAV)* and *Area Cover (G)* responses relative to the un-refined analysis (Figs. S4, S5). This was particularly noticeable in Renosterveld over the first winter (W1) where no treatment response was detected prior to the removal of over-represented species (Figs. S4, S5). However, despite these improvements, substantial disagreement between *Area Cover (UAV)* and *Area Cover (G)* responses remained at the Fynbos site after the removal of over-represented species from the ground-based analysis.

The disagreement between Fynbos *Area Cover (UAV)* and *Area Cover (G)* response patterns indicated that UAV-based data had detected vegetation changes which were undetected using ground-based measures at this site. Considering the identification of increased disagreement between *Area Cover (UAV)* and *Area Cover (G)* introduced by graminoid ground cover estimates at this site (Table 3), we tested the potential for the 'coarsely measured' graminoids to mask underlying Fynbos responses, by removing them from the ground-based analysis. Removing the problematic graminoids measurements from the ground-based analysis still resulted in the observation of low responsiveness of *Area Cover (G)* in remaining Fynbos species (Figs. S6, S7), indicating that graminoids were not masking underlying response patterns. By logical extension we concluded that the responsiveness to rainfall detected in Fynbos by UAVs (e.g., *Area Cover (UAV)*) was attributed to the graminoids, but that the ground-based cover estimates for this group had failed to detect their responses (see previous analysis of graminoids in van Blerk et al. 2021a, b showing no response).

'Vegetation NDVI' and 'shrub NDVI'

Within-canopy spectral changes detected from UAVs indicated stronger winter seasonality in Renosterveld vegetation under normal rainfall conditions. Here, *Vegetation NDVI* signals in Renosterveld displayed generally larger winter increases and summer declines than Fynbos (Fig. 8c). Furthermore, *Vegetation NDVI* signals were significantly more responsive to changes in rainfall seasonality in Renosterveld compared to Fynbos (Fig. 9c).

Shrub NDVI signals from each site showed similar patterns to the *Vegetation NDVI*. *Shrub NDVI* values for *Passerina obtusifolia,* in Renosterveld, were highly responsive to changes in seasonal

Table 2 Species with overrepresented ground measurements

Species	Species dominance: Contribution to total *Area Cover (G)* per plot (%)	Relationship between species dominance and plot *Area Cover (G)* over-estimation	Reason for overestimation
Wahlenbergia nodosa (Fynbos)	21 ± 9	$R^2 = 0.55$	Highly branched, diffuse canopy with reduced leaves
Thesium strictum (Renosterveld)	18 ± 11	$R^2 = 0.72$	Highly branched, diffuse canopy, absence of green leaves
Anthospermum gallioides (Renosterveld)	12 ± 11	$R^2 = 0.44$	Highly branched, diffuse canopy with reduced leaves
Microdon polygaloides (Renosterveld)	11 ± 5	$R^2 = 0.50$	Occurred in dense overlapping patches of individuals and underneath larger shrubs

*Note high R^2 values indicate strong plot area cover overestimation introduced by species

Table 3 Influence of growth form dominance (i.e., contribution to total *Area Cover (G)* per plot (%)) on disagreement between UAV and ground-based area cover measures. n = 12 plots per site

Growth form	Growth form dominance vs residual SE (i.e., disagreement)	
	Fynbos R^2	Renosterveld R^2
Woody resprouters	0.048	0.012
Graminoids	**0.683**	0.091
Perennial seedlings	0.026	0.137
Geophytes and bulbs	0.002	0.039
Prostrate resprouters	0.250	0.002
Annuals biennials and herbs	0.007	0.062

Note high R^2 values indicate strong disagreement between plot *Area Cover (G)* and *Area Cover (UAV)* introduced by growth-form

rainfall availability during all seasonal periods while *Agathosma capensis,* in Fynbos was not responsive (Figs. 8d, 9d). These findings closely mirror previous findings for these species based on ground-based volume changes (reported in Fig. 3 van Blerk et al. 2021a, b). Despite the differences in recovery patterns and responsiveness to treatments between sites, there was limited direct statistical support for differences in the magnitude and direction of treatment effects between these species.

'PlotNDVI'

Plot NDVI was the most highly integrated measure of vegetation recovery because it encompassed both changes in vegetation *Area Cover (UAV)* and within-canopy vegetation spectral changes (i.e., *Vegetation* NDVI) (Figs. 8a, 9a). However, *'Plot NDVI'* changes most closely mirrored the changes in *Area Cover (UAV)*, whereas *Vegetation NDVI* had a comparatively weaker influence. Fynbos and Renosterveld sites both showed strong winter seasonality under winter rainfall conditions while reduced rainfall seasonality muted or reversed seasonal '*Plot NDVI'* changes (Figs. 8a, 9a).

'Volume', 'height' and 'count'

Volume (Fig. 8e) patterns mirrored that of *Area Cover (G)* (Fig. 8f). Although ground-measured had the advantage of obtaining 3D measurements, this did not have much significance in terms of the patterns captured by these measurements because the influence of *Height* on *Volume* was low. Height (Fig. 8g) and count (Fig. 8h) showed strong natural seasonality in both sites although responses to treatments were inconsistent (Fig. 9g, h).

See Tables S1–S4 for full output stats tables.

Discussion

Our multi-year experiment, in the Cape Floristic Region of South Africa, monitored the responsiveness of post-fire shrubland recovery patterns to experimentally altered rainfall seasonality using repeated UAV and ground-based observations. UAV-based, multi-spectral imagery enabled the detection of

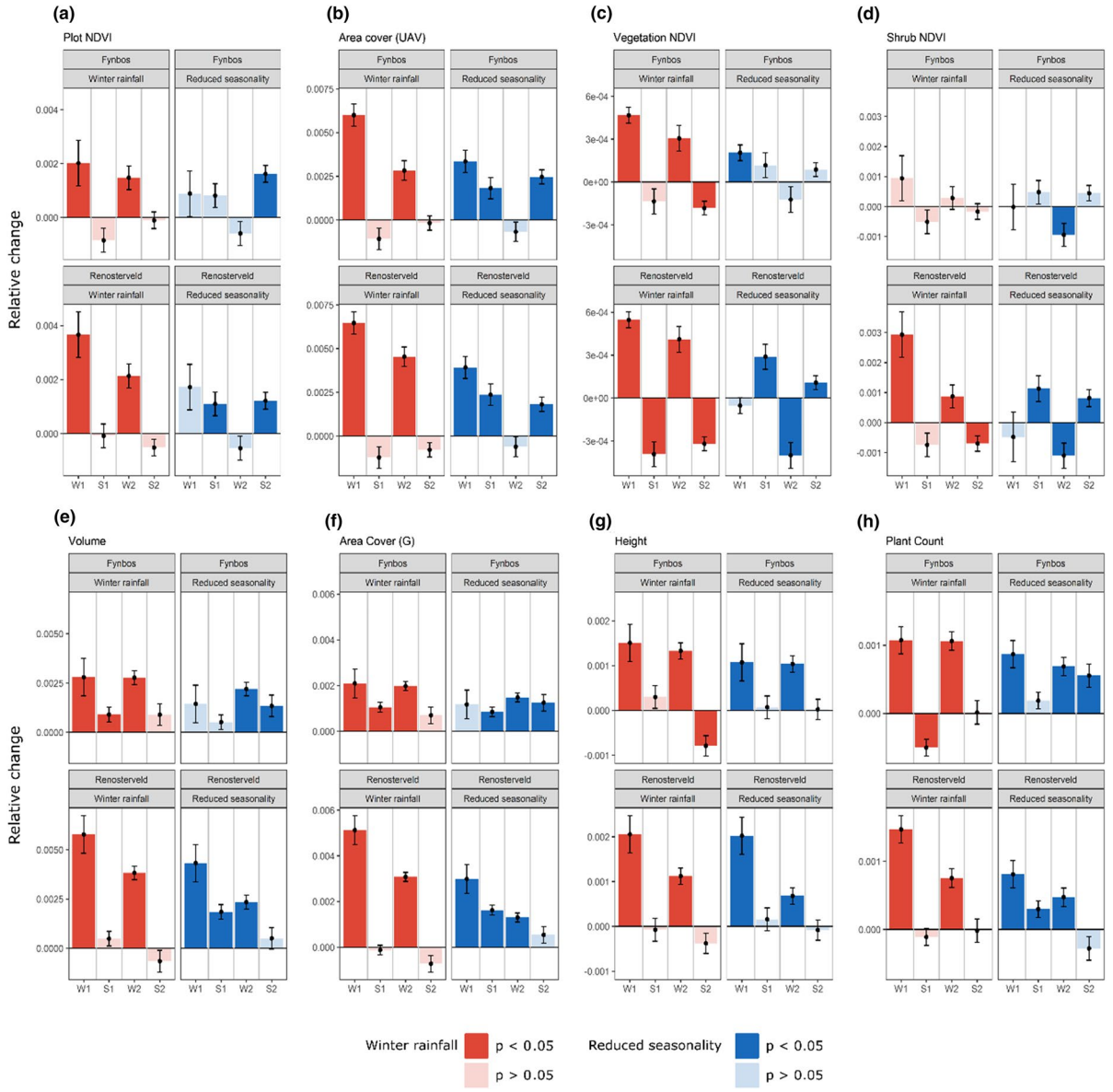

Fig. 8 Seasonal post-fire vegetation recovery patterns under contrasting rainfall seasonality treatments (i.e., winter rainfall and reduced seasonality). Points (mean) and error bars (SE) represent relative changes in ground and UAV-based measures over successive post-fire seasons: Winter 1 (W1), Summer 1 (S1), Winter 2 (W2), Summer 2 (S2). Shrub NDVI results (d) are based on *Agathosma capensis* in Fynbos and *Passerina obtusifolia* in Renosterveld

high-resolution vegetation changes at the patch-scale, improving on ground-based measures in terms of spatial resolution, coverage, and sensitivity. However, we highlighted the potential challenges in obtaining reliable measures of vegetation change from repeated multispectral images and emphasised the importance of adaptive relative radiometric image normalisation. Further, we demonstrated how a critical assessment

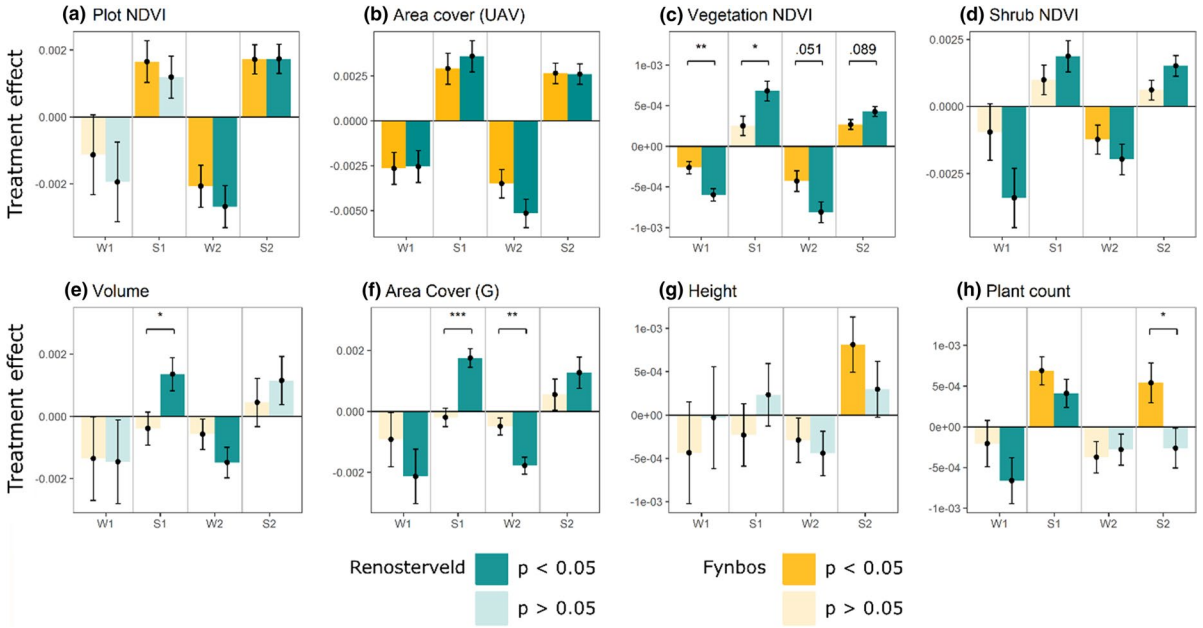

Fig. 9 Treatment responses to altered rainfall seasonality in Fynbos and Renosterveld sites for successive post-fire seasons: Winter 1 (W1), Summer 1 (S1), Winter 2 (W2), Summer 2 (S2). W1 and W2 represent the responses to a reduction in winter rainfall. S1 and S2 represent responses to increases in summer rainfall. Treatment effects are calculated as the difference in magnitude or direction of seasonal changes between winter rainfall and reduced seasonality plots. Statistical results for seasonal treatment effects are displayed for each season *p < 0.05, **p < 0.01, ***p < 0.001

of the relationships between UAV and ground-based measurements helped to refine our analyses. The careful integration of UAV and ground-based monitoring approaches proved to be highly complementary in our investigation. Our integrated findings pointed to strong coupling of post-fire recovery and rainfall in fertile, Renosterveld shrublands and relatively weaker coupling in neighbouring, nutrient-poor Fynbos shrublands (van Blerk et al. 2021a, b). These findings are consistent with previous ground-based observations at the site, which included individual species growth responses. However, UAVs also updated our understanding of the complexity of rainfall responses at the Fynbos site and helped to identify potential moisture coupling in the graminoid growth forms which was previously undetected using ground measurements. The apparent difference in sensitivity to rainfall between neighbouring Fynbos and Renosterveld shrublands highlights the potential for edaphic factors to mediate post-fire shrubland community sensitivity to rainfall. This mechanism could influence shrubland sensitivity to rainfall across edaphic boundaries at the regional scale in the CFR. Taken together our study demonstrated the effectiveness of using UAV-mounted, multispectral cameras in detecting ultra-fine-scale climate responses in early post-fire shrubland communities.

UAVs are powerful tools for observing fine-scale vegetation changes and have rapidly been adopted by ecologists (Anderson and Gaston 2013; Mathews and Jensen 2013; Malek et al. 2014; Pajares et al. 2015; Pádua et al. 2020), however, new users who are not remote sensing specialists, should avoid using a black-box approach to analysing UAV-based data (Rasmussen et al. 2016; Duffy et al. 2018; Buters et al. 2019). For example, while the spatial resolution of multi-spectral orthomosaic imagery from UAVs was high, converting these data into reliable measures of change over time required that repeated imagery was also radiometrically consistent over time. Temporal radiometric distortion is a key factor limiting remotely sensed change detection (Teillet 1986; Hall et al. 1991; Bao et al. 2012; Zhou et al. 2016), particularly where ultra-fine-scale patterns are the focus of detection. Our interrogation of imagery spectral data revealed substantial temporal radiometric distortion

even after following careful data capture normalisation protocols provided by the manufacturer. While we show that natural landscape features can be used successfully to conduct relative radiometric normalisation, this possibility is strongly dependent on the presence of such features in the environment being surveyed (e.g. evergreen shrubs, stable soils) and may be best applied in post-fire shrubland environments. If no stable soil value or vegetation value exists in the landscape, our proposed RRN methodology would not be applicable. Therefore, including permanent, multi-functional ground control points (e.g., Han et al. 2019) would ideally replace the organic (bare soil and dense, evergreen vegetation) PIFs used in our methodology. We also recommend including RGB imagery in UAV-based surveys. The ability to visually verify that multi-spectral vegetation indices represent real patterns is invaluable.

Our study highlighted the inherent challenges associated with "ground-truthing" of remotely sensed data (Zhou 1996), since both ground and UAV-derived measurements were subject to their own limitations and measured non-identical features of vegetation. For example, despite the excessive detail of our ground-based measurements, it was still logistically necessary to simplify individual plant canopy shapes corresponding to the widest and highest points each plant. These ground-based measures thus lacked the resolution to capture complex within-canopy changes occurring within these simplified shapes. UAV based measures were more sensitive to complex changes in vegetation cover but could not detect vegetation height differences or plants that were obscured from vision by taller plants and overlapping canopies. The practical advantages and limitations associated with ground and UAV-based monitoring approaches were thus dependent on the specific application or investigation. The efficiency of UAVs in quantifying integrated community responses (i.e., including all plants present) to rainfall over larger spatial scales was clear compared to ground-based measures. While our experiment only focused on key focal plots (due to the limitations of ground-based measures), the focal area of image-based data extraction could easily be scaled up, particularly with integrated community data (e.g. vegetation NDVI) which can be extracted from imagery using automated processes. Despite the advantages in describing integrated community changes, our captured imagery from UAVs was not conducive to identifying fine-scale demographic changes and species-level detail, to the same degree as ground-based measures. Only larger shrubs which were sufficiently isolated from other plantscould be measured independently. Despite this limitation, the response patterns of dominant shrubs *A. capensis* and *P. obtusifolia* (i.e. shrub NDVI) to treatment effects were highly comparable using UAV versus ground-based measures (see van Blerk et al. 2021a, b). While this worked for specific species, here the ground-based approach is clearly advantageous for less easily detectable species.

Taken together, our study highlighted the advantages in carefully integrating traditional and UAV-based techniques (Nagai et al. 2020) to better our understanding of dynamic post-fire recovery processes. Despite their differences, critically investigating the relationships between UAV and ground-based measurements was highly valuable for identifying areas of disagreement, which could then be investigated further. This approach clearly improved our understanding of the data and resulted in a refined analysis. Advancements in post-fire monitoring will rapidly advance our understanding of the impact of climate for these sensitive, hard-to-detect vegetation processes which may be formative for future vegetation states.

Acknowledgements Funding was generously provided by the NRF (93380 to AGW and 119125 to RA) and ACCESS groups (114696). Thank you to the Plant Conservation Unit for their contribution to the establishment of the Drie Kuilen rainfall manipulation experiment. JJvB was supported by a UCT Science Faculty Scholarship. We are grateful to the NCC and the Drie Kuilen Nature Reserve for providing access and support. Thank you to the many field assistants who were eager to help throughout the research process.

Author contributions JJvB, AGW, MTH, RA and JS conceptualized the research. JJvB, MTH and AGW collected the data. JJvB processed the data and wrote the manuscript, with contributions from AGW, MTH, RA and JS.

Funding Funding was provided by National Research Foundation (Grant Nos. 93380, 119125), National Research Foundation (ACCESS) (Grant No. 114696).

Data availability The data used during the current study are available from the corresponding author on reasonable request.

Declarations

Conflict of interest The authors have no relevant financial or non-financial interests to disclose.

References

Altwegg R, West A, Gillson L, Midgley GF (2014) Impacts of climate change in the Greater Cape Floristic Region. In: Allsopp N, Colville F, Verboom GA (eds) Fynbos: ecology, evolution, and conservation of a megadiverse region. Oxford University Press, New York, pp 299–320

Anderson K, Gaston KJ (2013) Lightweight unmanned aerial vehicles will revolutionize spatial ecology. Front Ecol Environ 11:138–146

Aplin P (2005) Remote sensing: ecology. Prog Phys Geogr 29(1):104–113

Baena S, Moat J, Whaley O, Boyd DS (2017) Identifying species from the air: UAVs and the very high resolution challenge for plant conservation. PLoS ONE 12:e0188714

Bao N, Lechner AM, Fletcher A, Mulligan D, Mellor A, Bai Z (2012) Comparison of relative radiometric normalization methods using pseudo-invariant features for change detection studies in rural and urban landscapes. J Appl Remote Sens 6:063578

Bergh NG, Verboom GA, Rouget M, Cowling RM (2014) Vegetation types of the greater cape floristic region. In: Allsopp N, Colville JF, Verboom GA (eds) Fynbos: ecology, evolution, and conservation of a megadiverse region. Oxford University Press, Oxford, pp 1–26

Bond WJ, Van Wilgen BW (2012) Fire and plants, vol 14. Springer, New York

Bradshaw PL, Cowling RM (2014) Landscapes, rock types, and climate of the Greater Cape Floristic Region. In: Allsopp N, Colville JF, Verboom GA (eds) Fynbos: ecology, evolution, and conservation of a megadiverse region. Oxford University Press, Oxford, pp 26–46

Buters TM, Bateman PW, Robinson T, Belton D, Dixon KW, Cross AT (2019) Methodological ambiguity and inconsistency constrain unmanned aerial vehicles as a silver bullet for monitoring ecological restoration. Remote Sens 11:1180

Cunliffe AM, Brazier RE, Anderson K (2016) Ultra-fine grain landscape-scale quantification of dryland vegetation structure with drone-acquired structure-from-motion photogrammetry. Remote Sens Environ 183:129–143

Du Y, Teillet PM, Cihlar J (2002) Radiometric normalization of multitemporal high-resolution satellite images with quality control for land cover change detection. Remote Sens Environ 82:123–134

Duffy JP, Cunliffe AM, DeBell L, Sandbrook C, Wich SA, Shutler JD, Myers-Smith IH, Varela MR, Anderson K (2018) Location, location, location: considerations when using lightweight drones in challenging environments. Remote Sens Ecol Conserv 4:7–19

Fernández-Guisuraga JM, Calvo L, Suárez-Seoane S (2022) Monitoring post-fire neighborhood competition effects on pine saplings under different environmental conditions by means of UAV multispectral data and structure-from-motion photogrammetry. J Environ Manage 305:114373

Ghazal M, Al Khalil Y, Hajjdiab H (2015) UAV-based remote sensing for vegetation cover estimation using NDVI imagery and level sets method. In 2015 IEEE international symposium on signal processing and information technology (ISSPIT), IEEE, pp 332–337

Gitas I, Mitri G, Veraverbeke S, Polychronaki A (2012) Advances in remote sensing of post-fire vegetation recovery monitoring—a review. Remote Sens Biomass-Princ Appl 1:334

Grime JP et al (2000) The response of two contrasting limestone grasslands to simulated climate change. Science 289:762–765

Hall FG, Strebel DE, Nickeson JE, Goetz SJ (1991) Radiometric rectification: toward a common radiometric response among multidate, multisensor images. Remote Sens Environ 35:11–27

Han X, Thomasson JA, Xiang Y, Gharakhani H, Yadav PK, Rooney WL (2019) Multifunctional ground control points with a wireless network for communication with a UAV. Sensors 19:2852

Keeley JE (2012) Fire in Mediterranean climate ecosystems—a comparative overview. Israel J Ecol Evol 58:123–135

Keeley JE, Fotheringham CJ, Baer-Keeley M (2005) Factors affecting plant diversity during post-fire recovery and succession of mediterranean-climate shrublands in California, USA. Divers Distrib 11:525–537

Kröel-Dulay G, Ransijn J, Schmidt IK, Beier C, De Angelis P, De Dato G, Penuelas J (2015) Increased sensitivity to climate change in disturbed ecosystems. Nat Commun 6:1–7

Malek S, Bazi Y, Alajlan N, AlHichri H, Melgani F (2014) Efficient framework for palm tree detection in UAV images. IEEE J Select Top Appl Earth Observ Remote Sens 7:4692–4703

Mathews A, Jensen J (2013) Visualizing and quantifying vineyard canopy LAI using an unmanned aerial vehicle (UAV) collected high density structure from motion point cloud. Remote Sens 5:2164–2183

Moreno JM, Zuazua E, Pérez B, Luna B, Velasco A, Resco de Dios V (2011) Rainfall patterns after fire differentially affect the recruitment of three Mediterranean shrubs. Biogeosciences 8:3721–3732

Mucina L, Rutherford MC (2006) The vegetation of South Africa, Lesotho and Swaziland. South African National Biodiversity Institute

Nagai S, Nasahara KN, Akitsu TK, Saitoh TM, Muraoka H (2020) Importance of the collection of abundant ground-truth data for accurate detection of spatial and temporal variability of vegetation by satellite remote sensing. Biogeochem Cycles 1:223–244

Nelson ZJ, Weisberg PJ, Kitchen SG (2013) Influence of climate and environment on post-fire recovery of mountain big sagebrush. Int J Wildl Fire 23:131–142

Odum P (1969) The strategy of ecosystem development. Science 164:262–270

Otsu N (1979) A threshold selection method from gray-level histograms. IEEE Trans Syst Man Cybern 9:62–66

Pádua L, Guimarães N, Adão T, Sousa A, Peres E, Sousa JJ (2020) Effectiveness of sentinel-2 in multi-temporal post-fire monitoring when compared with UAV imagery. ISPRS Int J Geo Inf 9:225

Pajares G (2015) Overview and current status of remote sensing applications based on unmanned aerial vehicles (UAVs). Photogramm Eng Remote Sens 81:281–330

QGIS Development Team (2009) QGIS geographic information system. Open source geospatial foundation. http://qgis.org

Rasmussen J, Ntakos G, Nielsen J, Svensgaard J, Poulsen RN, Christensen S (2016) Are vegetation indices derived from consumer-grade cameras mounted on UAVs sufficiently reliable for assessing experimental plots? Eur J Agron 74:75–92

Rutherford MC, Powrie LW, Husted LB, Turner RC (2011) Early post-fire plant succession in Peninsula Sandstone Fynbos: the first three years after disturbance. S Afr J Bot 77:665–674

Sankey TT, McVay J, Swetnam TL, McClaran MP, Heilman P, Nichols M (2018) UAV hyperspectral and lidar data and their fusion for arid and semi-arid land vegetation monitoring. Remote Sens Ecol Conserv 4:20–33

Teillet PM (1986) Image correction for radiometric effects in remote sensing. Int J Remote Sens 7:1637–1651

Tucker CJ (1979) Red and photographic infrared linear combinations for monitoring vegetation. Remote Sens Environ 8:127–150

van Blerk JJ, West AG, Altwegg R, Hoffman MT (2021a) Does a trade-off between growth plasticity and resource conservatism mediate post-fire shrubland responses to rainfall seasonality? New Phytol 230:1407–1420

van Blerk JJ, West AG, Altwegg R, Hoffman MT (2021b) Post-fire summer rainfall differentially affects reseeder and resprouter population recovery in fire-prone shrublands of South Africa. Sci Total Environ 788:147699

Veraverbeke S, Gitas I, Katagis T, Polychronaki A, Somers B, Goossens R (2012) Assessing post-fire vegetation recovery using red–near infrared vegetation indices: accounting for background and vegetation variability. ISPRS J Photogramm Remote Sens 68:28–39

Waite CE, van der Heijden GM, Field R, Boyd DS (2019) A view from above: unmanned aerial vehicles (UAV s) provide a new tool for assessing liana infestation in tropical forest canopies. J Appl Ecol 56:902–912

West AG, Dawson TE, February EC, Midgley GF, Bond WJ, Aston TL (2012) Diverse functional responses to drought in a Mediterranean-type shrubland in South Africa. New Phytol 195:396–407

Wilson AM, Latimer AM, Silander JA Jr (2015) Climatic controls on ecosystem resilience: postfire regeneration in the Cape Floristic Region of South Africa. Proc Natl Acad Sci USA 112:9058–9063

Zhou Q (1996) Ground truthing, how reliable is it. In: Proceedings of Geoinformatics' 96 Conference, West Palm Beach, FL pp 26–28

Zhou H, Liu S, He J, Wen Q, Song L, Ma Y (2016) A new model for the automatic relative radiometric normalization of multiple images with pseudo-invariant features. Int J Remote Sens 37:4554–4573